Unipolar assembly of zinc oxide rods manifesting polarity-driven collective luminescence

Ujjal K. Gautam[a,1], Masataka Imura[a], Chandra Sekhar Rout[b,2], Yoshio Bando[a], Xiaosheng Fang[a,1], Benjamin Dierre[c], Leonid Sakharov[d], A. Govindaraj[b], Takashi Sekiguchi[e], Dmitri Golberg[a], and C. N. R. Rao[b,1]

[a]International Center for Materials Nanoarchitectonics, National Institute for Materials Science Namiki 1-1, Tsukuba, Ibaraki 305-0044, Japan; [b]International Centre for Materials Science, Jawaharlal Nehru Centre for Advanced Scientific Research, Jakkur P.O., Bangalore 560 064, India; [c]Department of Physics, University of Trento, Via Sommarive 14, I-38050 Povo (Trento), Italy; [d]L. Sakharov, LeoKrut, 34 Hamilton Road 310, Arlington, MA 02474; and [e]Advanced Electronic Materials Center, National Institute for Materials Science, Namiki 1-1, Tsukuba, Ibaraki 305-0044, Japan

Oriented assemblies of small crystals forming larger structures are common in nature and crucial for forthcoming technologies as they circumvent the difficulties of structural manipulation at microscopic scale. We have discovered two distinctive concentric assemblies of zinc oxide rods, wherein each rod has an intrinsically positive and a negative polar end induced by the noncentrosymmetric arrangement of Zn and O atoms. All the rods in a single assembly emanate out of a central core maintaining a single polar direction. Due to growth along the two polar surfaces with different atomic arrangements, these assemblies are distinct in their intrinsic properties and exhibit strong UV luminescence in the exterior of Zn-polar assemblies, unlike the O-polar assemblies. Although novel applications can be envisioned, these observations suggest that hierarchical organization with respect to internal asymmetry might be widespread in natural crystal assemblies.

cathodoluminescence | crystal assembly

Spontaneous assembly of small crystals into organized structures is a process of transformation from disorder to order. Such processes are abundant in natural systems and are of fundamental importance because these constitute the basic building blocks in many inorganic or biomineralization processes (1–10). When assembling into larger systems, the constituent crystals orient themselves with respect to each other following certain specific criteria. The macroscopic shape of a skeletal plate of sea urchin is thus dictated by the crystallographic axis of calcite (6). By using peptides extracted from living organisms, oriented assemblies of nanoparticles can be obtained in vitro, too (7). Quantum-confined tetrahedra are the tiniest well-defined assemblies having four wurtzite arms built over a zinc blende core (8). Such assemblies lead to emergence of properties that are not directly related to the information encoded on each individual component, but are dependent on how these units are organized in space (1, 4).

A specially interesting situation may arise when a constituent in an assembly contains an element of asymmetry in its crystal structure. Wurtzite zinc oxide (ZnO) is one such system, where sequential stacking of Zn- and O-atomic layers, one on top of the other, along the crystallographic c axis gives rise to intrinsic polarity within the crystal with partial positive and negative charges along Zn- and O-terminated ends, respectively (Fig. 1) (11). In all assemblies and hierarchical structures of ZnO, a growth direction along this polar axis is usually maintained. What would be interesting to know is whether Nature goes a step further in assembling these systems, i.e., making the crystallographic axis as well as the polar direction relevant. This would lead to the existence of an additional symmetry, such as organization of dipoles inside the assembly, as shown schematically in Fig. 1 C and D, for instance. Herein, we report the mesoscopic concentric assemblies of ZnO rods, where all the rods in a single assembly grow along either positive or negative polar ends. Unipolar growth leads to distinct optical emission patterns from these

assemblies at a microscopic level. These observations demonstrate that the self-similarity observed in natural and biological systems extends to crystal assemblies, not in shape alone, but also in internal properties. Unique applications, such as developing a transiently charged crystal assembly due to the pyroelectric nature of ZnO (such as those in Fig. 1C) can now be envisioned (12, 13).

Results and Discussion

The unipolar Al doped ZnO rod assemblies were obtained by a hydrothermal procedure by reacting zinc acetate, aluminum nitrate, and sodium hydroxide dissolved in mixed solvent of water and ethanol (1:1). X-ray diffraction (XRD) measurements confirmed purity of the sample and its wurtzite ZnO structure. A SEM image of the ZnO assemblies is shown in Fig. 1D, revealing that each assembly has a common core from which the rods grow out. The reaction product contained two distinct types of assemblies, the major fraction (yield ~70–80%) consisting of rods, all with a smooth tip (Fig. 1E). The average diameter of the smooth tip rods is 0.36 μm, whereas average length is 3.10 μm. In the other fraction, the rods are larger with a mean diameter and length of 0.64 μm and 6.5 μm, respectively, and have sharp, pencil-like tips (Fig. 1 F and G). Fig. 1J shows the angular orientation of the rods within the two assemblies. The smooth tip assemblies are sparse in density with interrod angles of 20°–40°, the angles in the sharp tip assembly being 10°–20°. Thus, the sharp tip assemblies are 15–20 times heavier than the smooth tip assemblies. We also observe the presence of some freestanding rods in the reaction product. Fig. 1H shows a rod whose ends resemble the two kinds of tips in the assemblies.

Transmission electron microscope (TEM) investigations revealed that the ZnO rods are single-crystalline in nature. Fig. 2 B and C show a typical selected-area electron diffraction (SAED) pattern and a high-resolution TEM (HRTEM) image, respectively, of the ZnO arm marked in Fig. 2A. The results are identical for smooth tip rods, too, and the growth direction of individual ZnO rods is [0001] in both the assemblies. Energy dispersive X-ray spectroscopy measurements show the Al content to vary within 2–3.5% in the different rods, whereas the elemental composition of rods is uniform throughout.

The tip morphology, size, and angular orientations establish the distinct nature of the two assemblies, and it appeared that the differences might originate from the polar direction associated
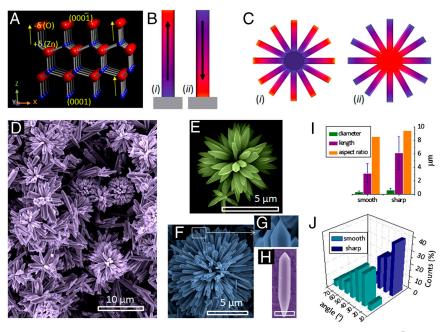
Fig. 1. (*A*) Crystal structure of wurtzite ZnO. The unit cell is dominated by four low Miller index surfaces: the nonpolar $(10\bar{1}0)$ and $(11\bar{2}0)$ surfaces and the polar zinc-terminated (0001)-Zn and oxygen-terminated $(000\bar{1})$-O surfaces. Arrows indicate the polar direction of Zn-O bonds. (*B*) (*i* and *ii*) Schematic showing the orientation of polarity in two ZnO rods grown along the $(000\bar{1})$ and 0001 directions within the *c*-crystallographic axis, respectively. (*C*) Schematic representation of two possible assemblies of ZnO rods. Besides a possibility of being randomly oriented, all rods in an assembly may also orient along (*i*) the negative or (*ii*) positive polar direction, making the two identical looking assemblies intrinsically different. (*D*) SEM image of the ZnO assemblies. (*E* and *F*) High magnification images of the two types of ZnO assemblies having smooth and sharp tips, respectively. (*G*) Enlarged view of the fraction framed in (*F*). (*H*) A freestanding ZnO rod having a sharp and a smooth tip (scale bar = 500 nm). (*I*) Bar diagram depicting approximate diameters, lengths, and aspect ratios, and (*J*) the distribution of angles between two consecutive arms in an assembly.

with the nanorods. We systematically investigated convergent beam electron diffraction (CBED) patterns acquired from the sharp and smooth tip structures in order to unambiguously determine the polarity (14). Fig. 2*A*1 and *D*1 show typical experimental CBED patterns acquired from sharp and smooth tips, respectively, along the $[10\bar{1}0]$ zone axis having inversion symmetry. The central disk (symmetrical in intensity) in the patterns corresponds to the 0000 diffraction spot. The upper and lower disks are opposite in contrast and correspond to the (0002) and $(000\bar{2})$ planes, respectively. Dynamic simulation of the CBED patterns was performed using the Bloch-wave program (Fig. 2*A*2 and *D*2) (15). Agreement of the experimental patterns with the simulated ones confirmed that the sharp ZnO tips grow along the positive [0001] direction (i.e., Zn-polar direction), whereas the smooth tips grow along the negative $[000\bar{1}]$ direction (i.e., O-polar direction). Thus the two types of assemblies are structurally unique. The smooth tip assemblies grow only in the O-polar direction, whereas the sharp tip assemblies grow along the Zn-polar direction.

The significance of the unipolar ZnO assemblies can be illustrated from two distinct viewpoints. First, the two assemblies are related by a unique and simple relation; i.e., one assembly can be converted to the other by a single symmetry operation wherein each rod is rotated in the center and about its diameter by 180°. Similar analogies can be found in molecular structures, such as in stereoisomers, where two enantiomers that rotate polarized light in opposite directions are related by mirror symmetry. Therefore, the ZnO assemblies might possess properties that are complementary in nature. In addition, these assemblies are also unique among an extremely large variety of ZnO nanostructures that have emerged as a key component for energy harvesting and green technologies (16–19). Versatility in ZnO morphology arises from the fundamental propensity to grow in one crystallographic axis forming nanorods and nanobelts as well as the long-range interactions forming nanorings (20). The present findings demonstrate the possibility that one-dimensional ZnO

rods can be grown in exclusively unipolar directions. This is crucial for distinct properties as the Zn- and the O-polar faces involve different growth mechanisms.

ZnO assemblies with similar morphology can be obtained by many other techniques, and therefore their growth is not specific to Al doping and hydrothermal synthesis (21). On the basis of the rod diameter and the angle between the rods (Fig. 1 *I* and *J*), the core size of the O-polar and the Zn-polar assemblies should be 6 and 23 μm, respectively, which is clearly not realistic. In some SEM images, tapering of the ZnO rods near the core (Fig. 2*F*) and secondary growth (Fig. 2*G*) were observed. We suggest that the nucleus triggering the polarity control is actually much smaller in size and must have several unipolar facets on its surface. Among such assemblies, ZnO tetrapods have the simplest geometry and originate from the octahedral multiple twins (22). More highly branched, but symmetric structures have been suggested to originate from crystal twining, too (23). On the contrary, orientation selection continuously varies between different crystallographic directions during dendritic growth (24). However, despite extensive research, the growth mechanism of loosely regular mesocrystals, like the present unipolar assemblies, is largely unknown (25). We attempted to isolate the intermediate structures by quenching the reaction at different time intervals. This was not conclusive, as quenching leads to secondary nucleation decorating the already existing structures. Thus, the unipolar assemblies can neither be described as a self-assembly nor as a single crystal, and their exact growth mechanism remains an open question.

We observed distinct polarity-induced luminescence properties of the Zn- and O-terminated assemblies by using cathodoluminescence (CL) spectroscopy. As compared to the conventional phololuminescence spectroscopy, CL has the advantage of higher spatial resolution up to few nanometers and is suitable for studying a single assembly among many (26). Fig. 3*A* shows CL spectra acquired from Zn-polar and O-polar assemblies using an accelerating voltage of 10 kV and a 2,000-pA probe current. Both the
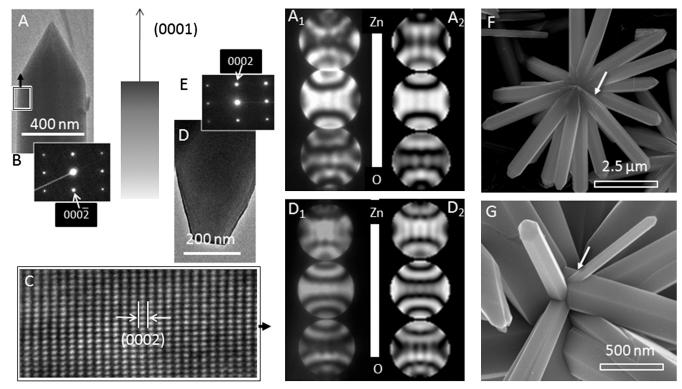
Fig. 2. TEM images and the corresponding SAED patterns of (*A* and *B*) a sharp and (*D* and *E*) a smooth tip ZnO arm. (*C*) HRTEM image acquired from the region marked with a rectangle in *A*. (*A1* and *D1*) Experimental CBED patterns acquired from the rods shown in *A* and *D*, respectively. Corresponding simulated CBED patterns are shown in *A2* and *D2*. The diffraction patterns are sensitive to the specimen thickness, and the best match was found by using 125 nm and 165 nm for the sharp and the smooth tip rods, respectively. (*F*) SEM image of an assembly where the core is visible. Arrow indicates tapering of the rods. (*G*) Another assembly showing secondary growth of a ZnO rod marked by an arrow.

spectra have a sharp UV emission at ~390 nm and a broad defect emission centered at ~600 nm, but the Zn-polar assembly shows a 4-nm blue shift of the UV emission band. It is significant that the distribution of luminescence across a single structure is different in the two types of rods, although the overall spectra are similar. Fig. 3 *B–D* show CL mapping images corresponding to emission wavelengths of 390 nm and 600 nm for a Zn-polar assembly. Fig. 3 *E–G* show the same for an O-polar assembly. The Zn-polar rods have stronger UV emission at the tips and at the base. The visible emission is strongest in the middle region. In the case of O-terminated rods, the UV emission is strongest at the base, whereas the visible emission is somewhat uniform. Investigation of a large number of Zn- and O-polar assemblies confirmed such luminescence behavior. Fig. 3*H* depicts a series of CL spectra taken across an O-polar ZnO arm (indicated in Fig. 3*E*) showing that the emission intensity (UV in this case) may vary up to 400% within a single structure. These images and spectra illustrate how the luminescence pattern within each rod in an assembly varies smoothly and continually. To demonstrate this systematic variation, we acquired CL spectra from 10 equally spaced positions across a rod, starting from the tip (point #1) to the base (point #10), in different assemblies, and extracted the intensities of the UV and visible emission at each position. Fig. 3 *I* and *J* display the variation of luminescence across the Zn- and the O-polar assemblies. These CL images and the plots demonstrate that these ZnO rods are unique and also that this feature leads to the emergence of properties in a collective manner in the two types of assemblies, rendering them distinguishable.

Similar variations in CL intensities across a nanorod have been observed in aligned ZnO nanorod arrays recently (27). The change in luminescence at various positions can be attributed to the presence of different types of defects across a rod (28). We believe that a dynamic process involving two interdependent growth

factors accounts for similarity in spatial emission patterns in all the rods within a particular type of assembly. An important factor is the difference in growth kinetics on the Zn and the O faces as the molecular ZnO precursors undergo transformations on these faces with different reaction mechanisms (29). The second factor is the surface of a growing crystal that acts as a substrate for the next layer of ZnO, which, with continuous consumption of the reactants, evolves constantly in its characteristics such as surface roughness, morphology, and defect concentration. These traits are retained in the crystal in the form of native defects and affect the growth kinetics, in addition to reactant concentrations, as the growth proceeds further. *SI Text* shows results of Monte Carlo simulations on ZnO crystal growth, where the surface roughness, a measure of internal defects in this instance, constantly evolves with the progress of the reaction. This mechanism of mutual feedback, wherein crystal surface and reactant concentrations affect the growth kinetics, which in turn changes the nature of the surface, leads to gradual variation in properties within each ZnO rod (Fig. 3*K*).

The spontaneous formation of concentric, unipolar assemblies of ZnO rods is of great interest in understanding growth and polarity-dependent properties. Two oppositely polar assemblies prepared under identical conditions develop entirely distinct optoelectronic properties, due to the unique spatial organization of the individual rods. Such polarity control could be a general natural phenomenon and can occur in assemblies of others materials, too, such as those reported for ferroelectric, ferromagnetic, piezoelectric materials, etc., having an element of asymmetry (30, 31).

Materials and Methods

Synthesis of the Unipolar Assemblies. The unipolar ZnO 1D assemblies were synthesized by a hydrothermal procedure by using $Zn(CH_3COO)_2 \cdot 2H_2O$ (600 mg) as the Zn precursor, $Al(NO_3)_3 \cdot 9H_2O$ (30 mg) as the Al source, and NaOH (2.2 g) as the corresponding hydrolyzing agent. The dissolved
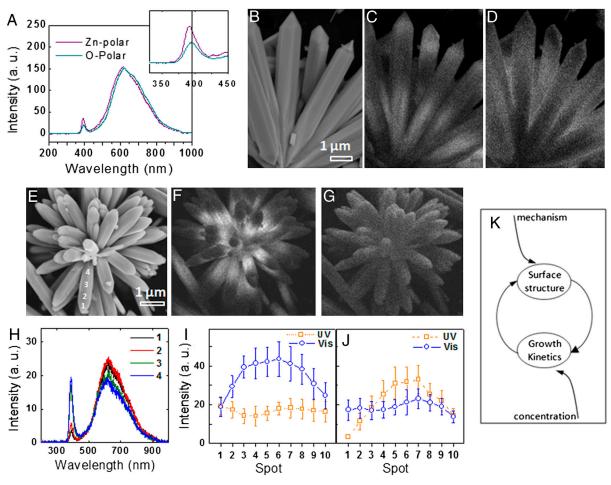
Fig. 3. (*A*) CL spectra acquired from an O-polar and a Zn-polar assembly. (*Inset*) Highlights the UV emissions. (*B–D*) SEM and CL images corresponding to emissions at 390 nm and 600 nm, respectively, for a Zn-polar assembly. Similar images recorded on an O-polar assembly are shown in *E–G*. (*H*) CL spectra taken along a ZnO arm, seen in *E* showing that the visible emission remains consistent while the UV emission intensity gradually changes. (*I* and *J*) Plots showing systematic variation of UV and visible emission intensities across Zn-polar and O-polar assemblies (from tip to the base), respectively. (*K*) Schematic showing the various factors, e.g., reaction mechanism, reactant concentrations and interdependent growth kinetics, and surface structures, that instill systematic variation in properties inside each assembly.

chemicals in 40-mL mixed solvent of water and ethanol (1:1) was treated in ultrasonic water bath for 30 min. The solvothermal synthesis was conducted for 24 h using a Teflon-lined autoclave (80% filling) in a hot-air oven that was preheated to 200 °C. After the reaction, the white products were washed with deionized water and ethanol and dried at 60 °C in vacuum for 24 h. For details of the synthesis, refer to *SI Text*.

Characterization. As-prepared Al-doped ZnO assemblies were characterized by using X-ray diffraction (SEIFERT, 3000TT with Cu Kα, $\lambda = 0.15418$ nm radiation), field-emission SEM (JSM-6700F), and a TEM (JEM-3000F) equipped with an energy-dispersive X-ray spectroscope (EDS). Simulated CBED patterns were obtained by many-beam dynamical calculations. The intensity calculation is based on the Bloch-wave formulation of dynamical theory (15). After the structural and chemical examinations, spatially resolved CL measurements on individual ZnO assemblies were carried out. CL spectra were collected with a high-resolution CL system at 10-kV accelerating voltage and at a constant current density of 2,000 pA at room temperature, by using

Ultra-High Vacuum SEM and a Gemini electron gun (Omicron) equipped with a CL system (32). The vacuum of the specimen chamber was maintained at 10^{-11} mbar.

Supporting Information. Detailed synthesis procedure for the unipolar ZnO assemblies, estimation of their CL properties, XRD pattern, EDS spectra and EDS mapping images, HRTEM image, low-magnification CL mapping image, and Monte Carlo simulation of surface roughness of a growing ZnO crystal as a function of precursor concentration are described in *SI Text*.

1. Whitesides GM, Grzybowski B (2002) Self-assembly at all scales. *Science* 295:2418–2421.
2. Söllner C, et al. (2003) Control of crystal size and lattice formation by starmaker in otolith biomineralization. *Science* 302:282–286.
3. Cölfen H, Mann S (2003) Higher-order organization by mesoscale self-assembly and transformation of hybrid nanostructures. *Angew Chem Int Edit* 42:2350–2365.
4. Mann S (2009) Self-assembly and transformation of hybrid nano-objects and nanostructures under equilibrium and non-equilibrium conditions. *Nat Mater* 8:781–792.
5. Ruiz JMG, García EM, Hyde ST (2009) Morphogenesis of self-assembled nanocrystalline materials of barium carbonate and silica. *Science* 323:362–365.

6. Donnay G, Pawson DL (1969) X-ray diffraction studies of echinoderm plates. *Science* 166:1147–1150.
7. Sugawara A, et al. (2006) Self-organization of oriented calcium carbonate/polymer composites: Effects of matrix peptide isolated from the exoskeleton of a crayfish. *Angew Chem Int Edit* 45:2876–2879.
8. Manna L, Milliron DJ, Meisel A, Scher EC, Alivisatos AP (2003) Controlled growth of tetrapod-branched inorganic nanocrystals. *Nat Mater* 2:382–386.
9. Tian ZR, Liu J, Voigt JA, Mckenzie B, Xu H (2003) Hierarchical and self-similar growth of self-assembled crystals. *Angew Chem* 42:413–417.
10. Kulp EA, Switzer JA (2007) Electrochemical biomineralization: The deposition of calcite with chiral morphologies. *J Am Chem Soc* 129:15120–15121.

11. Yu YM, Liu BG (2008) Contrasting morphologies of O-rich ZnO epitaxy on Zn- and O-polar thin film surfaces: Phase-field model. *Phys Rev B* 77:195327.

12. Pyroelectricity is an inherent property of polar materials. Upon cooling or heating, the atomic positions in the crystal changes slightly such that polarization of the materials changes. The two ends perpendicular to the polar axis develop equal but opposite charges. The sign of the charge at a given surface is determined by the direction of polarity of the crystal and can be either positive or negative, depending on whether the material is cooled down or warmed up. The charges developed in this way may take several minutes to disipate (13). Because all rods in the concentric ZnO assemblies grow in a single polar direction, the entire spherical exterior of the assembly is expected to develop either positive or negative charge when subjected to a temperature change.

13. Ehre D, Lavert E, Lahay M, Lubomirsky I (2010) Water freezes differently on positively and negatively charged surfaces of pyroelectric materials. *Science* 327:672–675.

14. Wang ZL, Kong XY, Zuo JM Induced growth of asymmetric nanocantilever arrays on polar surfaces. *Phys Rev Lett* 91:185502.

15. Tsuda K, Tanaka M (1999) Refinement of crystal structural parameters using two-dimensional energy-filtered CBED patterns. *Acta Crystallogr* A55:939–954.

16. Wang ZL (2009) ZnO nanowire and nanobelt platform for nanotechnology. *Mater Sci Eng B Adv* 64:33–71.

17. Wang ZL, Song J (2006) Piezoelectric nanogenerators based on zinc oxide nanowire arrays. *Science* 312:242–246.

18. Wang ZL (2008) Towards self-powered nanosystems: From nanogenerators to nanopiezotronics. *Adv Funct Mater* 18:3553–3557.

19. Huang MH, et al. (2001) Room-temperature ultraviolet nanowire nanolasers. *Science* 292:1897–1899.

20. Kong XY, Wang ZL (2003) Spontaneous polarization-induced nanohelixes, nanosprings, and nanorings of piezoelectric nanobelts. *Nano Lett* 3:1625–1631.

21. Zhang Y, Mu J (2007) Controllable synthesis of flower- and rod-like ZnO nanostructures by simply tuning the ratio of sodium hydroxide to zinc acetate. *Nanotechnology* 18:075606.

22. Nishio K, Isshiki T, Kitano M, Shiojiri M (1997) Structure and growth mechanism of tetrapod-like ZnO particles. *Philos Mag A* 76:889–904.

23. Ma YY, et al. (2008) Twin-crystal nature of the single-crystal-like branched Cu_2O particles. *J Phys Chem C* 112:13405–13409.

24. Haxhimali T, Karma A, GonZales F, Rappaz M (2005) Orientation selection in dendritic evolution. *Nat Mater* 5:660–664.

25. Cölfen H, Antonietti M (2005) Mesocrystals: Inorganic superstructures made by highly parallel crystallization and controlled alignment. *Angew Chem Int Edit* 44:5576–5591.

26. Yacobi BG, Holt DB (1990) *Cathodoluminescence Microscopy of Inorganic Solids* (Plenum Press, New York).

27. Chung TF, Zapien JA, Lee ST (2008) Luminescent properties of ZnO nanorod arrays grown on Al:ZnO buffer layer. *J Phys Chem C* 112:820–824.

28. Zeng H, et al. (2010) Blue luminescence of ZnO nanoparticles based on non-equilibrium processes: Defect origins and emission controls. *Adv Funct Mater* 20:561–572.

29. Dem'yanets LN, Kostomarov DV, Kuz'mina IP (2002) Chemistry and kinetics of ZnO growth from alkaline hydrothermal solutions. *Inorg Mater* 38:124–131.

30. Rørvik PM, Grande T, Einarsrud MA (2009) Hierarchial $PbTiO_3$ nanostructures grown on $SrTiO_3$ substrates. *Cryst Growth Des* 9:1979–1984.

31. Yao WT, et al. (2006) Architectural control syntheses of CdS and CdSe nanoflowers, branched nanowires, and nanotrees via a solvothermal approach in a mixed solution and their photocatalytic property. *J Phys Chem B* 110:11704–11710.

32. Dierre B, Yuan XL, Ohashi N, Sekiguchi T (2008) Effects of specimen preparation on the cathodoluminescence properties of ZnO nanoparticles. *J Appl Phys* 103:083551.